11. Spencer PD, Roth KS. Effects of succinylacetone on amino acid uptake in the rat kidney. *Biochem Med Metabol Biol* 1987;37:101–109.
12. Foreman JW, Bowring MA, Lee J, et al. Effect of cystine dimethylester on renal solute handling and isolated renal tubule transport in the rat: a new model of the Fanconi syndrome. *Metabolism* 1987;36:1185–1191.
13. Bakker WH, Albert R, Bruns C, et al. [^{111}In-DTPA-D-Phe^1]octreotide, a potential radiopharmaceutical for imaging of somatostatin receptor-positive tumors: synthesis, radiolabeling and in vitro validation. *Life Sci* 1991;49:1583–1591.
14. Wall DA, Maak T. Endocytic uptake, transport and catabolism of proteins by epithelial cells. *Am J Physiol* 1985;248:C12–C20.
15. Duncan JR, Welch MJ. Intracellular metabolism of indium-111-DTPA-labeled receptor targeted proteins. *J Nucl Med* 1993;34:1728–1738.
16. Rogulski J, Pacanis A. Effects of maleate on CoA metabolism in rat kidney. *Biochem Nephrol Curr Probl Clin Biochem* 1978;8:406–415.
17. Neuhaus OW. Acetoacetate does not prevent maleate-induced proteinuria in rats. *Nephron* 1989;53:83–84.
18. Hysing J, Ostensen J, Tolleshaug H, Kiil F. Effect of maleate on tubular protein reabsorption in dog kidneys. *Renal Physiol* 1987;10:338–351.
19. De Jong M, Breeman WAP, Bernard HF, et al. Evaluation in vitro and in rats of ^{161}Tb-DTPA-octreotide, a somatostatin analog with potential for intraoperative scanning and radiotherapy. *Eur J Nucl Med* 1995;22:608–616.
20. Verani RR, Brewer ED, Ince A, et al. Proximal tubular necrosis associated with maleic acid administration to the rat. *Lab Invest* 1982;46:79–88.

Detecting Infection and Inflammation with Technetium-99m-Labeled Stealth® Liposomes

Wim J.G. Oyen, Otto C. Boerman, Gert Storm, Louis van Bloois, Emile B. Koenders, Roland A.M.J. Claessens, Roos M. Perenboom, Daan J.A. Crommelin, Jos W.M. van der Meer and Frans H.M. Corstens

Departments of Nuclear Medicine and Internal Medicine, University Hospital Nijmegen, Nijmegen, The Netherlands; and Institute for Pharmaceutical Science, Department of Pharmaceutics, Utrecht University, Utrecht, The Netherlands

The performance of ^{99m}Tc Stealth® liposomes was investigated in various rat models. **Methods:** Preformed polyethyleneglycol-containing liposomes with encapsulated reduced glutathione, were radiolabeled using the lipophilic ^{99m}Tc-HMPAO. The labeled liposomes were intravenously administered to rats with focal *S. aureus* or *E. coli* infection, or turpentine-induced inflammation. For comparison, Tc-99m-nanocolloid- and ^{99m}Tc-labeled nonspecific IgG were tested. In rats with *Pneumocystis carinii* pneumonia (PCP), Tc-99m-liposomes were directly compared to In-111 labeled nonspecific IgG. **Results:** Technetium-99m-liposomes accumulated in the infectious and inflammatory muscle foci over 24 hr (0.59% injected dose per gram tissue (%ID/g) for *E. coli;* 0.98 %ID/g for *S. aureus;* 1.18 %ID/g for turpentine). Abscess-to-muscle ratios increased to values as high as 24.0, 41.7 and 44.5 for the respective models at 24 hr postinjection. Technetium-99m-liposomes visualized the foci as early as 1 hr postinjection. Technetium-99m-IgG visualized *S. aureus* infection, but abscess-to-muscle ratios and abscess uptake at the later time points were significantly lower. Technetium-99m-nanocolloid failed to visualize any of the muscle foci. In PCP however, ^{99m}Tc-liposomes did not show preferential localization in the infection. The control agent ^{111}In-IgG showed a significant, two-fold increase in lung uptake. **Conclusion:** Technetium-99m-Stealth® liposomes preferentially accumulated in abscesses, leading to very high target-to-nontarget ratios. This property appears to be related to a process based on uptake of long-circulating particles. In a specific type of infection, i.c. PCP, ^{99m}Tc-liposomes did not accumulate in diseased lung tissue, thus mimicking the in vivo behavior of labeled leukocytes.

Key Words: polyethyleen glycol; immunoglobulin; technetium-99m-liposomes; indium-111-IgG; infection imaging; inflammation; *Pneumocystis carinii*

J Nucl Med 1996; 37:1392–1397

Imaging infection and inflammation at early time points with convenient radiopharmaceuticals approaches the clinician's concept of optimal imaging of infectious and inflammatory disease (*1*). Since none of the currently available radiopharmaceuticals is ideal with regard to biodistribution, pharmacokinetics or accumulation in a focus, both preclinical and clinical efforts are made to develop an agent that meets these goals. One of the promising, new agents for scintigraphic detection of infection and inflammation is radiolabeled liposomes. Liposomes consist of lipid bilayer membranes, enclosing aqueous compartments in which aqueous labels can be entrapped. In the past liposomes have been widely studied for achieving controled drug delivery and for imaging purposes (*2–5*). However, these conventional liposomes are rapidly cleared from the circulation by phagocytic cells of the mononuclear phagocyte system (MPS) (*6*). Therefore, their use for diagnostic imaging is limited as the efficient MPS uptake competes with accumulation at the target site. Development of new liposome formulations characterized by prolonged circulation time was a significant step forward. The so-called sterically stabilized, or Stealth® (Liposome Technology, Inc., Menlo Park, CA), liposomes have been shown to preferentially localize at diseased sites (*7,8*). In Stealth® liposomes, polyethylene glycol (PEG) is incorporated in the phospholipid bilayer, thereby drastically reducing the recognition of the liposomes by the MPS and thus increasing circulatory half-life. Recently, we have demonstrated excellent targeting of experimental focal infection with ^{111}In-labeled Stealth® liposomes (*9*). When abscess accumulation and biodistribution are favorable, a ^{99m}Tc label is to be preferred over ^{111}In. In this study, we evaluated ^{99m}Tc-labeled Stealth® liposomes. Applicability of the ^{99m}Tc label and the performance in several infection and inflammation models were studied. The performance of ^{99m}Tc-liposomes was compared to other reagents used in clinical practice.

Received May 17, 1995; revision accepted Aug. 18, 1995.
For correspondence or reprints contact: Wim J.G. Oyen, MD, University Hospital Nijmegen, Department of Nuclear Medicine, P.O. Box 9101, 6500 HB Nijmegen, The Netherlands.

MATERIALS AND METHODS

Animal Models

Muscle Infection/Inflammation. A calf muscle abscess was induced in young, male, randomly-bred Wistar rats (body weight 200–220 g). After ether anesthesia, approximately 2×10^8 colony-forming units (CFU of *Staphyloccoccus aureus* or 1×10^9 CFU of *Escherichia coli* in 0.1 ml 50:50% suspension of autologous blood and normal saline was injected in the left calf muscle (*10*). Sterile inflammation was induced by injection of 0.15 ml of turpentine in the left calf muscle of ether-

anaesthetized rats. Twenty-four hours after the inoculation, when swelling of the muscle was apparent, the respective radiopharmaceuticals were injected via the tail vein.

Pneumocystis Carinii Pneumonia. Young female, randomly-bred Sprague-Dawley rats (body weight 150–175 g) were immunosuppressed by weekly subcutaneous injections of 25 mg hydrocortisone and an 8% protein restricted diet. Amoxicillin (1 mg/ml) was added to the drinking water to prevent bacterial infections. *Pneumocystis carinii* pneumonia (PCP) was induced by close cohabitation with *P. carinii*-infected rats for 4 wk. Viral co-infection was excluded by regular serological screening on common rodent viruses. PCP infection was confirmed and bacterial co-infection excluded by microscopic examination of Giemsa-stained smears of the cut surface of the lung.

Radiopharmaceuticals

Technetium-99m-Labeled Liposomes. We used partially hydrogenated egg-phosphatidylcholine with an iodine value of 40 (PHEPC) (*11*). The PEG 1900 derivative of distearoylphosphatidylethanolamine (PEG-DSPE) was donated by Liposome Technology, Inc. (Menlo Park, CA) and prepared as described previously (*12*). Cholesterol and glutathione were obtained commercially.

A chloroform/methanol mixture (10/1, v/v) containing PEG-DSPE, PHEPC and cholesterol was prepared in a molar ratio of 0.15:1.85:1. A lipid film was formed by rotary evaporation followed by high vacuum to remove residual organic solvent. The film was hydrated at room temperature in 50 m*M* glutathione in HEPES buffer (10 m*M* HEPES, 135 m*M* NaCl at pH 7.4) at an initial phospholipid concentration of 120 m*M*. The resulting dispersion was passed through a microfluidizer. Unentrapped glutathione was removed by gel filtration. The particle size distribution was determined by dynamic light scattering. The mean size of the liposomes was 80–100 nm.

Preformed glutathione-containing liposomes were labeled by transporting ^{99m}Tc as a lipophilic ^{99m}Tc-hexamethylpropyleneamine oxime (HMPAO) complex through the bilayer. The ^{99m}Tc-HMPAO is subsequently irreversibly trapped in the internal aqueous phase due to reduction by the encapsulated glutathione (*13*). One milligram HMPAO was incubated with 2.5 GBq ^{99m}Tc-pertechnetate. The liposomes were incubated for 15 min at room temperature with 1 MBq ^{99m}Tc-HMPAO per μmole phospholipid. Labeling efficiency was between 60 and 70%. Removal of unencapsulated ^{99m}Tc-HMPAO was achieved by gel filtration on a Econo Pac 10DG column (Bio-Rad, Richmond, CA) with 5% glucose solution as the eluent.

A commercially available kit for ^{99m}Tc-IgG (Technescan-HIG, Mallinckrodt Medical, Petten, The Netherlands) was labeled with ^{99m}Tc according to the manufacturer's instructions. Labeling efficiency as determined by instant thin layer chromatography (ITLC) was higher than 95%.

A commercially available kit for ^{99m}Tc-nanocoll (Solco nanocoll, Sorin Biomedica, Vercelli, Italy) was labeled with ^{99m}Tc according to the manufacturer's instructions. The particle size, as checked by dynamic light scattering, was 80–90 nm.

Human, nonspecific polyclonal IgG (^{111}In-IgG) was conjugated to diethylenetriaminepentaacetic bicyclic anhydride (bicyclic DTPA) as described by Hnatowich et al. (*14*) and labeled with ^{111}In-chloride. Labeling efficiency as determined by ITLC was higher than 95%.

Study Design

Biodistribution Studies. Twenty-four hours after *S. aureus* inoculation (15 rats), *E. coli* inoculation (15 rats) or turpentine injection (15 rats) in the left calf muscle, the animals were injected with 1 MBq of ^{99m}Tc-liposomes in the tail vein. Analogously, 24 hr after *S. aureus* inoculation a group of 15 rats was injected with 1 MBq of ^{99m}Tc-IgG. At 2, 8 and 24 hr postinjection, five rats of each group were killed with 30 mg intraperitoneally-injected phenobarbital. Blood was obtained by cardiac puncture. Following cervical dislocation, tissues (infected left calf muscle, right calf muscle, liver, spleen, kidney, small bowel, right femur and bone marrow from the right femur) were dissected, weighed and their activity was measured in a shielded well-type gamma counter. To correct for physical decay and to permit calculation of the uptake of the radiopharmaceuticals in each organ as a fraction of the injected dose, aliquots of the injected dose were counted simultaneously. Abscess-to-muscle and abscess-to-blood ratios were calculated.

Five PCP-infected and five noninfected, weight- and sex-matched control rats were injected via the tail vein with a mixture of 1 MBq ^{99m}Tc-liposomes and 0.4 MBq ^{111}In-IgG. Twenty-four hours later, all rats were killed with 30 mg intraperitoneally-injected phenobarbital. Blood was obtained by cardiac puncture. Following cervical dislocation, the lungs and a muscle sample from the right calf were obtained, weighed and their activity was measured in a shielded well-type gamma counter. To correct for physical decay and for contribution of ^{111}In to the ^{99m}Tc counts, and to permit calculation of the uptake of the radiopharmaceuticals in the organs as a fraction of the injected dose, aliquots of the injected doses were counted simultaneously. Lung-to-muscle and lung-to-blood ratios were calculated.

Imaging Studies. Twenty-four hours after *S. aureus* infection, groups of three rats were injected intravenously via the tail vein with 10 MBq ^{99m}Tc-liposomes, 10 MBq ^{99m}Tc-nanocoll or 10 MBq ^{99m}Tc-IgG. Analogously, 24 hr after *E. coli* infection or intramuscular turpentine injection (as described above), groups of three rats were injected intravenously through the tail vein with 10 MBq ^{99m}Tc-liposomes.

The rats were anaesthesized with a halothane/nitrousoxide/oxygen mixture and placed prone on a single-head gamma camera equipped with a parallel-hole, low-energy collimator. Each group of rats was imaged at 5 min and 0.75, 2, 4, 6, 10–12 and 24 hr after injection. Images (300,000 counts per image) were obtained and stored in a 256 × 256 matrix.

The scintigrams were analyzed by drawing regions of interest over the abscess, over the noninfected contralateral calf muscle (used as a background region), over the heart (representing blood-pool activity) and over the whole animal. Abscess-to-background ratios and percentage residual activity in the abscess (abscess-to-whole body ratio) were calculated.

Statistical Analysis

All mean values are given as percent injected dose per gram tissue (%ID/g) or ratios ± 1 s.e.m. Statistical analysis was performed using one-way analysis of variance (ANOVA). The level of significance was set at $p < 0.05$.

RESULTS

Twenty-four hours after injection in the left calf muscle, inflammation was observed at inspection and palpation in all three models. Turpentine caused the most significant inflammatory process: gross swelling and induration without pus formation. *S. aureus* infection caused swelling and induration and pus formation. The inflammatory activity caused by *E. coli* infection was the mildest compared to the other two models with relatively mild swelling and induration and little pus formation.

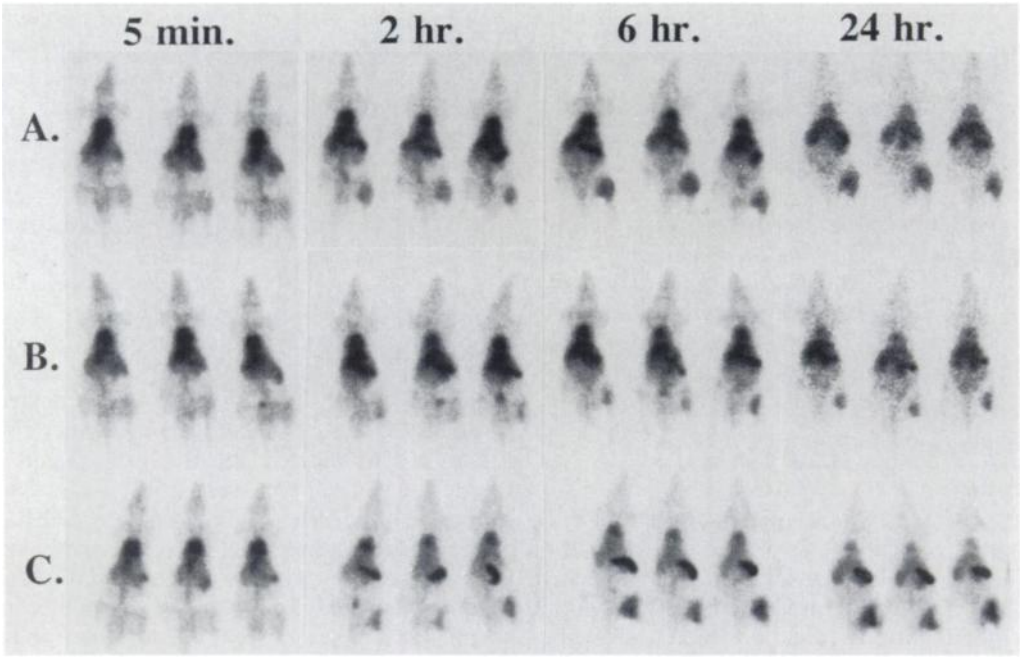

FIGURE 1. Images of ^{99m}Tc-liposomes at 5 min and 2, 6 and 24 hr after injection in rats with (A) *S. aureus* infection, (B) *E. coli* infection or (C) turpentine-induced inflammation.

Figure 1 shows the scintigraphic images of ^{99m}Tc-liposomes at various time points in the three muscle inflammation/infection models. In all models, the abscess was clearly visualized as early as 2 hr postinjection. An over-time increment of the relative uptake in the abscess was noted. Figure 2 shows the quantitative analysis of the images. There was a steady increase of the ^{99m}Tc-liposomes uptake in the abscess (Fig. 2A, 2B). The activity in the blood pool (represented by a region of interest over the heart) showed an initial half life of approximately 12 hr (Fig. 2C). Over 24 hr, 23.2 ± 0.9 %ID was excreted in urine.

The biodistribution data (Table 1) indicate an increase of activity in the abscess over time occuring in all three models: from 2 hr postinjection onwards a significant increase in abscess uptake, abscess-to-muscle ratios and abscess-to-blood ratios was observed ($0.001 < p < 0.01$). Compared to the uptake at 2 hr postinjection, absolute uptake in the abscess more than doubled, abscess-to-muscle ratios increased more than three-fold, and abscess-to-blood ratios increased more than eight-fold. Nevertheless, the abscess uptake of ^{99m}Tc-liposomes depended on the type of focal infection/inflammation. From 2 hr postinjection onwards, ^{99m}Tc-liposomes uptake in the *S. aureus* and turpentine abscess was significantly higher than that in the *E. coli* abscess ($p < 0.01$). Turpentine caused a relatively rapid accumulation in the abscess: at 8 hr postinjection, the abscess uptake was significantly higher in the turpentine abscess compared to the *S. aureus* abscess ($p < 0.01$). This difference was not observed at 24 hr postinjection. Since normal muscle uptake was low throughout the study, abscess-to-muscle ratios follow the same pattern as absolute abscess uptake, as indicated in Table 1. At 24 hr postinjection, abscess-to-muscle ratios in the *S. aureus, E. coli* and turpentine abscess were as high as 41.7 ± 4.1, 24.0 ± 4.5, and 44.5 ± 4.9, respectively. Abscess-to-blood ratios were only significantly different at 8 hr postinjection: turpentine > *S. aureus* > *E. coli* ($0.001 < p < 0.05$).

The biodistribution data in Table 2 show relatively low activity in liver (1–2 %ID/g) kidneys (2–3 %ID/g), lung (<1% %ID/g), bone marrow (<1% %ID/g) and bowel (<0.5% %ID/g). The spleen showed relatively high uptake (>12 %ID/g). When evaluating total organ uptake, liver and spleen activity, being the primary target organs for Stealth® liposomes, account for the most substantial physiological organ uptake (10%–20% ID and 6%–8% ID, respectively).

Technetium-99m-IgG, a clinically used reagent, localized in *S. aureus* infection, even at early time points. However, as shown in Table 1, abscess uptake decreased over time and became significantly lower than ^{99m}Tc-liposomes in the same model at 24 hr postinjection (0.49 ± 0.04 %ID/g versus 0.98 ± 0.08 %ID/g, respectively, $p < 0.001$). As shown in Table 1, abscess-to-muscle ratios were significantly lower at all time points than the respective ratios obtained with ^{99m}Tc-liposomes in the *S. aureus* model (at 24 hr postinjection, 11.8 ± 1.4 and 41.7 ± 4.1, respectively, $p < 0.0001$). Abscess-to-blood ratios were in the same range at all time points, due to faster clearance of ^{99m}Tc-IgG from blood and whole body. Technetium-99m-IgG cleared faster from the blood pool (initial half life of approximately 5 hr) and was more rapidly excreted (over 24 hr, 49.0 ± 0.8 %ID was excreted in urine). Quantification of the imaging studies were in line with biodistribution data: after an initial increase of abscess-to-background ratios, ^{99m}Tc-IgG is washed out from the abscess. Technetium-99m-IgG finally showed an abscess-to-background ratio of 4.9 ± 1.0, compared to 11.8 ± 1.0 after ^{99m}Tc-liposomes injection ($p < 0.001$). As shown in Table 2, the most striking differences in organ distribution between liposomes and IgG were the high activity in the spleen of ^{99m}Tc-liposomes and the high renal uptake of ^{99m}Tc-IgG. Liver, lung, bone marrow and bowel uptake were similar.

Despite the similar size compared to the labeled liposomes, ^{99m}Tc-nanocolloid failed to image focal infection. Nanocolloid was cleared rapidly from the circulation by the MPS. Abscess-to-background ratios, calculated from the scintigrams, were very low. Immediately after intravenous injection, the ratios were only 1.7 ± 0.1, as a result of increased local perfusion. Thereafter, the reagent failed to visualize the abscesses. Abscess-to-background ratio decreased to values 1.2. In contrast,

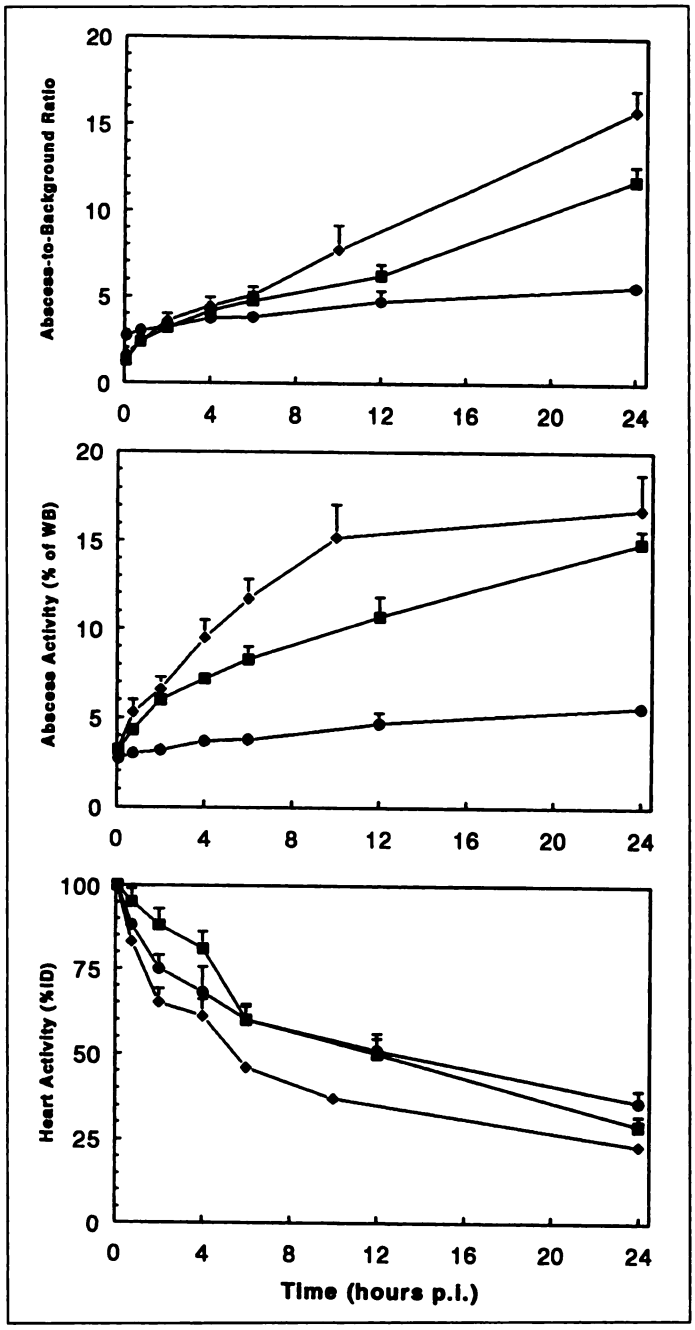

FIGURE 2. Quantitative analysis (mean ± s.e.m.) of the scintigraphic images of rats injected with ^{99m}Tc-liposomes after *S. aureus* (■) or *E. coli* (●) inoculation or intramuscular turpentine (◆) injection. (A) Abscess-to-background ratios. (B) Retained activity in the abscess as percentage of residual whole-body activity. (C) Blood clearance, represented by activity in the heart region. Activity measured 5 min postinjection was considered as 100%.

when using ^{99m}Tc-liposomes in the *S. aureus* model, abscess-to-background ratios steadily increase over time and reaching values as high as 11.8 ± 1.0 at 24 hr postinjection ($p < 0.0001$).

In the PCP model, severe *P. carinii* infestation in the lungs was histologically confirmed. However, no increased ^{99m}Tc-liposomes uptake in the infected lungs could be observed. As shown in Table 3, absolute uptake, lung-to-muscle and lung-to-blood ratios were nearly identical to the ratios in noninfected animals. In contrast, the control agent ^{111}In-IgG showed significant accumulation in the infected lungs, compared to noninfected control animals (lung uptake 2.13 ± 0.41 %ID/g versus 1.02 ± 0.06 %ID/g, respectively, $p < 0.01$).

DISCUSSION

The present study shows that ^{99m}Tc-labeled Stealth® liposomes accumulate significantly in infectious and inflammatory lesions over time. High absolute uptake (up to 1 %ID/g), abscess-to-muscle (up to 40) and abscess-to-blood ratios (higher than 1) are observed in the various models of experimental muscle infection and inflammation. Biodistribution showed relatively low uptake in other tissues, except for marked splenic accumulation (approximately 15% ID/g). This splenic uptake is still much lower than that of non-PEGylated larger liposomes (39 %ID/g) (*5*). Also, bone marrow uptake may be lower for Stealth® liposomes (<1% ID/g, for non-PEGylated liposomes >5 %ID/g). Blood clearance and uptake in other organs of Stealth® and non-PEGylated ^{99m}Tc-labeled liposomes are similar (*5*). Excretion of radioactivity is also similar for both formulations (23 %ID for Stealth®, 30 %ID for non-PEGylated over 24 hr). Overall, targeting of the infectious focus with ^{99m}Tc-Stealth® liposomes is at least as good or even better than that of ^{99m}Tc-non-PEGylated liposomes (two-fold increase of absolute abscess uptake and abscess-to-blood ratios, similar abscess-to-muscle ratios). Further improvement may be achieved by optimizing size and blood clearance (*15*).

Labeling Stealth® liposomes with ^{99m}Tc or ^{111}In also causes differences. At 24 hr, absolute abscess uptake of ^{111}In-liposomes in the *S. aureus* model is significantly higher compared to ^{99m}Tc-liposomes: 1.93 ± 0.54 %ID/g and 0.98 ± 0.08 %ID/g, respectively (*9*). However, due to different kinetics (i.e., faster clearance of the ^{99m}Tc agent from blood and background) abscess-to-muscle ratios are two-fold higher for ^{99m}Tc-liposomes and abscess-to-blood ratios are very similar (*9*). Excretion of ^{111}In-liposomes is less than 5% over 24 hr, excretion of ^{99m}Tc-liposomes 23%. In the biodistribution, only the very low renal uptake is in favor of the ^{111}In-liposomes (less than 1 %ID/g compared to almost 3 %ID/g for ^{99m}Tc-liposomes).

Whether or not this inflammation is induced by a microorganism is irrelevant as illustrated by the accumulation in various types of muscle inflammation. This indicates that infection is not crucial and that the microorganisms are not responsible for abscess uptake. The uptake and accumulation of the liposomes appeared to correlate with the intensity of inflammatory response of a focus. *E. coli* infection, with the mildest inflammatory response at visual insection and palpation, shows abscess uptake of up to 0.6 %ID/g and abscess-to-muscle ratios of up to 24. In contrast, the more severe *S. aureus* infection has abscess uptake of up to 1.0 %ID/g and abscess-to-muscle ratios of over 40 at 24 hr after injection. Turpentine-induced inflammation causes uptake at least as high as the abscess uptake in *S. aureus* infection.

Apparently, blood clearance is more important than particle size for determining accumulation in inflammatory foci. Technetium-99m-nanocolloid, used in clinical practice for infection imaging (*16*), only showed a mild increase in flow without any accumulation in the *S. aureus* focus. However, size of the liposomes is an important issue in ^{99m}Tc-liposomes accumulation. In one control experiment the liposomes were stored at 4–8°C for 3 wk; their size increased to 600 nm during storage. These larger liposomes did not show accumulation in *E. coli* or *S. aureus* abscesses, but were rapidly cleared from circulation. Abscess-to-background ratios on the scintigrams were 1.5 or lower.

Technetium-99m-liposomes also compared favourably with ^{99m}Tc-IgG, a commercially available radiopharmaceutical for imaging infection and inflammation in humans (*17*). Both abscess uptake and abscess-to-muscle ratios were significantly higher for the labeled liposomes. Important factors are the

TABLE 1
Abscess, Muscle and Blood Activity (%ID/g ± s.e.m.) and Ratios (± s.e.m.) of Technetium-99m-Liposomes and Technetium-99m-IgG in Focal Calf Muscle Infection/Inflammation

	Time postinjection (hr)	^{99m}Tc-liposomes			^{99m}Tc-IgG
		S. aureus	*E. coli*	Turpentine	*S. aureus*
Abscess	2	0.45 ± 0.01	0.23 ± 0.02	0.46 ± 0.06	0.68 ± 0.02
	8	0.63 ± 0.07	0.36 ± 0.02	0.97 ± 0.06	0.60 ± 0.02
	24	0.98 ± 0.08	0.59 ± 0.10	1.18 ± 0.12	0.49 ± 0.04
Muscle	2	0.03 ± 0.001	0.04 ± 0.002	0.04 ± 0.002	0.08 ± 0.01
	8	0.03 ± 0.002	0.04 ± 0.002	0.03 ± 0.002	0.06 ± 0.004
	24	0.02 ± 0.001	0.03 ± 0.001	0.03 ± 0.001	0.04 ± 0.002
Blood	2	3.40 ± 0.02	2.78 ± 0.11	3.59 ± 0.03	3.04 ± 0.15
	8	2.07 ± 0.11	1.89 ± 0.08	1.98 ± 0.12	1.57 ± 0.05
	24	0.83 ± 0.04	0.65 ± 0.07	1.11 ± 0.08	0.61 ± 0.02
Abscess-to-muscle ratio	2	13.2 ± 0.5	5.6 ± 0.6	13.0 ± 1.9	8.8 ± 1.0
	8	18.6 ± 2.4	9.0 ± 0.9	40.5 ± 5.0	9.8 ± 0.5
	24	41.7 ± 4.1	24.0 ± 4.5	44.5 ± 4.9	11.8 ± 1.4
Abscess-to-blood ratio	2	0.1 ± 0.0	0.1 ± 0.0	0.1 ± 0.0	0.2 ± 0.0
	8	0.3 ± 0.0	0.2 ± 0.0	0.5 ± 0.0	0.4 ± 0.0
	24	1.2 ± 0.1	0.9 ± 0.1	1.1 ± 0.1	0.8 ± 0.1

relatively fast blood and whole-body clearance of ^{99m}Tc-IgG due to high renal uptake and urinary excretion. Compared to ^{99m}Tc-liposomes, the initial half life of ^{99m}Tc-IgG in the circulation is much shorter (12 versus 5 hr) and the excretion over 24 hr two-fold higher (23 %ID versus 49 %ID).

A remarkable aspect of ^{99m}Tc-liposomes is the failure of this formulation to detect PCP. While ^{111}In-IgG, known to be also clinically useful for detection of PCP (*18*), showed significant lung uptake in diseased rats, ^{99m}Tc-liposomes uptake did not differ from uptake in noninfected controls. However, this is not caused by an inability of liposomes to target pulmonary infection. Previous experiments showed high liposome uptake in *Klebsiella pneumoniae* lung infection (*8*). The causative microorganism seems to play a key role in this respect. It appears that liposomes show a very similar in vivo behavior compared to labeled leukocytes. While labeled leukocytes are excellent for fast detection of acute (bacterial) infection or inflammation, they also do not localize in PCP (*19*). Unfortunately, labeled leukocyte scintigraphy is not possible in a rat model.

CONCLUSION

When the analogy of ^{99m}Tc-liposomes and ^{99m}Tc-labeled leukocytes is confirmed in terms of performance in human studies, obvious advantages of the liposome formulation would be the continuous availability of a high-quality radiopharmaceutical that can be prepared easily without the need to handle blood. In patient care, labeled liposomes would then be an attractive agent to replace labeled leukocytes, especially in acute infectious disease. Further comparative studies in experimental infection are ongoing.

TABLE 2
Biodistribution of Technetium-99m-Liposomes in Focal Calf Muscle Infection/Inflammation (%ID/g ± s.e.m.)

	Time postinjection (hr)	^{99m}Tc-liposomes			^{99m}Tc-IgG
		S. aureus	*E. coli*	Turpentine	*S. aureus*
Liver	2	2.01 ± 0.32	1.97 ± 0.11	0.79 ± 0.06	1.00 ± 0.08
	8	1.94 ± 0.10	1.79 ± 0.21	0.92 ± 0.13	0.76 ± 0.03
	24	1.40 ± 0.04	1.32 ± 0.10	0.94 ± 0.13	0.45 ± 0.03
Spleen	2	11.53 ± 1.04	11.53 ± 0.81	18.46 ± 1.21	0.86 ± 0.10
	8	13.07 ± 1.79	12.78 ± 0.94	16.86 ± 2.00	0.61 ± 0.02
	24	12.49 ± 0.87	10.31 ± 1.22	16.26 ± 1.03	0.38 ± 0.03
Kidney	2	2.05 ± 0.17	2.16 ± 0.11	1.77 ± 0.12	5.72 ± 0.42
	8	2.27 ± 0.09	2.57 ± 0.13	1.96 ± 0.07	7.26 ± 0.27
	24	3.07 ± 0.08	2.92 ± 0.21	2.51 ± 0.08	7.06 ± 0.70
Lung	2	0.53 ± 0.13	0.79 ± 0.09	0.93 ± 0.05	0.96 ± 0.07
	8	0.63 ± 0.07	0.64 ± 0.02	0.52 ± 0.04	0.58 ± 0.01
	24	0.35 ± 0.03	0.26 ± 0.02	0.33 ± 0.02	0.32 ± 0.03
Bone marrow	2	0.94 ± 0.24	1.02 ± 0.11	—	0.85 ± 0.09
	8	0.85 ± 0.11	0.41 ± 0.18	—	0.56 ± 0.04
	24	0.32 ± 0.08	0.34 ± 0.05	—	0.29 ± 0.02
Bowel	2	0.38 ± 0.03	0.34 ± 0.03	0.38 ± 0.04	0.52 ± 0.11
	8	0.40 ± 0.05	0.42 ± 0.05	0.38 ± 0.04	0.27 ± 0.02
	24	0.37 ± 0.04	0.31 ± 0.02	0.40 ± 0.04	0.15 ± 0.00

TABLE 3

Pulmonary Uptake (%ID/g ± s.e.m.) and Ratios (± s.e.m.) of Technetium-99m-Liposomes and Indium-111-IgG 24 Hours after Injection of *Pneumocystis Carinii* Pneumonia in Rats and Noninfected Controls

	^{99m}Tc-liposomes*		^{111}In-IgG†	
	PCP	Noninfected	PCP	Noninfected
Lung uptake	0.98 ± 0.30	0.92 ± 0.08	2.13 ± 0.41	1.02 ± 0.06
Lung-to-blood ratio	0.4 ± 0.0	0.4 ± 0.0	0.7 ± 0.1	0.5 ± 0.0
Lung-to-muscle ratio	14.0 ± 2.3	12.7 ± 1.5	10.1 ± 2.7	4.3 ± 0.5

*No significant increase in pulmonary ^{99m}Tc-liposome uptake and ratios in PCP-infected rats compared to noninfected control animals.

†Significantly increased pulmonary ^{111}In-IgG uptake and ratios in PCP-infected rats compared to noninfected control animals ($p < 0.01$ for all values).

ACKNOWLEDGMENT

We thank Gerrie Grutters for expert technical assistance.

REFERENCES

1. Corstens FHM, van der Meer JWM. Chemotactic peptides: new locomotion for imaging of infection? *J Nucl Med* 1991;32:491–494.
2. Morgan JR, Williams LA, Howard CB. Technetium-labeled liposome imaging for deep-seated infection. *Br J Radiol* 1985;58:35–39.
3. O'Sullivan MM, Powell N, French AP, et al. Inflammatory joint disease: a comparison of liposome scanning, bone scanning and radiography. *Ann Rheum Dis* 1988;47:485–491.
4. Williams BD, O'Sullivan MM, Saggu GS, et al. Synovial accumulation of technetium-labeled liposomes in rheumatoid arthritis. *Ann Rheum Dis* 1987;46:314–318.
5. Goins B, Klipper R, Rudolph AS, et al. Biodistribution and imaging studies of technetium-99m-labeled liposomes in rats with focal infection. *J Nucl Med* 1993;34: 2160–2168.
6. Karlowsky JA, Zhanel GG. Concepts on the use of liposomal antimicrobial agents: applications for aminoglycosides. *Clin Infect Dis* 1992;15:654–667.
7. Gabizon A. Selective tumor localization and improved therapeutic index of anthracyclines encapsulated in long-circulating liposomes. *Cancer Res* 91992;52:891–896.
8. Bakker-Woudenberg IAJM, Lokerse AF, ten Kate MT, et al. Liposomes with prolonged blood circulation and selective localization in Klebsiella pneumoniae-infected lung tissue. *J Infect Dis* 1993;168:164–171.
9. Boerman OC, Storm G, Oyen WJG, et al. Sterically stabilized liposomes labeled with indium-111 for imaging focal infection in rats. *J Nucl Med* 1995;36:1639–1644.
10. Oyen WJG, Claessens RAMJ, Van der Meer J, Corstens FHM. Biodistribution and kinetics of radiolabeled proteins in rats with focal infection. *J Nucl Med* 1992;33:338–394.
11. Lang J, Vigo-Pelfrey C, Martin F. Liposomes composed of partially hydrogenated egg phosphatidylcholines: fatty acid composition, thermal phase behaviour and oxidative stability. *Chem Phys Lipids* 1990;53:91–101.
12. Woodle MC, Matthay KK, Newman MS, et al. Versatility in lipid compositions showing prolonged circulation with sterically stabilized liposomes. *Biochim Biophys Acta* 1992;1105:193–200.
13. Neirinckx RD, Burke JF, Harrison RC, et al. The retention mechanism of technetium-99m-HMPAO: intracellular reaction with glutathione. *J Cereb Blood Flow Metab* 1988;8:S4–S12.
14. Hnatowich DJ, Childs RL, Lanteigne D, Najafi A. The preparation of DTPA-coupled antibodies radiolabeled with metallic radionuclides: an improved method. *J Immunol Meth* 1983;65:147–157.
15. Litzinger DC, Buiting AM, van Rooijen N, Huang L. Effect of liposome size on the circulation time and intraorgan distribution of amphipathic poly(ethylene glycol)-containing liposomes. *Biochim Biophys Acta* 1994;1190:99–107.
16. Gericke M, Eckart L. Möglichkeiten und grenzen der nanokolloid-szintigraphie in der diagnostik von infektionen am bewegungsapparat. *Nucl Med* 1990;13:93–105.
17. Buscombe JR, Lui D, Ensing G, et al. Tc-99m-human immunoglobulin (HIG)—first results of a new agent for the localization of infection and inflammation. *Eur J Nucl Med* 1990;16:649–655.
18. Buscombe JR, Oyen WJG, Grant A, et al. Indium-111-labeled polyclonal human immunoglobulin: identifying focal infection in patients positive for human immunodeficiency virus. *J Nucl Med* 1993;34:1621–1625.
19. Alazraki NP. Radionuclide imaging in the evaluation of infections and inflammatory disease. *Radiol Clin North Am* 1993;31:783–794.

FIRST IMPRESSIONS: (ERRATUM)

Due to a production error, the images in the July *JNM* First Impressions, by Boren et al. were printed incorrectly. The corrected images and text are reprinted below.

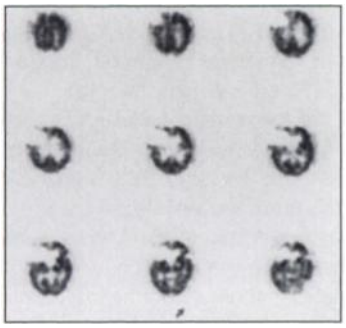

Figure 1.

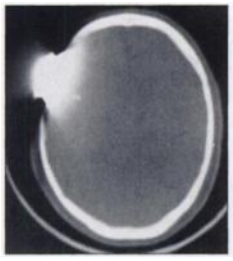

Figure 2.

Figure 3.

PURPOSE

A 71-yr-old man with a history of mild CVA in 1990 presented with clinical dementia. The patient was referred for brain SPECT imaging to rule out Alzheimer's disease. Figure 1 shows axial images of the brain with a round photopenic defect in the right frontal lobe that extends outside the cortex and into the cranium and soft tissues. Figures 2 and 3 depict axial CT images through the metal plate and a digital lateral skull film with the metal plate clearly demonstrated.

TRACER

Technetium-99m-HMPAO, 32 mCi (884 MBq)

ROUTE OF ADMINISTRATION

Intravenous

TIME AFTER INJECTION

90 minutes

INSTRUMENTATION

Picker Triple-Head Prism 3000 SPECT with ultra-high resolution, fanbeam collimation

CONTRIBUTORS

Edwin L. Boren, Jr., Christopher L. Cowan and Shirley G. Anderson

INSTITUTION

John L. McClellan Memorial Veterans Hospital, Little Rock, Arkansas